Kinetics of the Thermal Oxidation of Ir(100) toward IrO2 Studied by Ambient-Pressure X-ray Photoelectron Spectroscopy

Novotny, Zbynek ; Tobler, Benjamin ; Artiglia, Luca ; Fischer, Martin ; Schreck, Matthias ; Raabe, Jörg ; Osterwalder, Jürg

Abstract: Using time-lapsed ambient-pressure X-ray photoelectron spectroscopy, we investigate the thermal oxidation of single-crystalline Ir(100) films toward rutile IrO2(110) in situ. We initially observe the formation of a carbon-free surface covered with a complete monolayer of oxygen, based on the binding energies of the Ir 4f and O 1s core level peaks. During a rather long induction period with nearly constant oxygen coverage, the work function of the surface changes continuously as sensed by the gas phase O 1s signal. The sudden and rapid formation of the IrO2 rutile phase with a thickness above 3 nm, manifested by distinct binding energy changes and substantiated by quantitative XPS analysis, provides direct evidence that the oxide film is formed via an autocatalytic growth mechanism that was previously proposed for PbO and RuO2.

DOI: https://doi.org/10.1021/acs.jpclett.0c00914

THE JOURNAL OF PHYSICAL CHEMISTRY Letters

pubs.acs.org/JPCL Letter

Kinetics of the Thermal Oxidation of Ir(100) toward IrO_2 Studied by Ambient-Pressure X-ray Photoelectron Spectroscopy

Zbynek Novotny,* Benjamin Tobler, Luca Artiglia, Martin Fischer, Matthias Schreck, Jörg Raabe, and Jürg Osterwalder*

Cite This: J. Phys. Chem. Lett. 2020, 11, 3601−3607 Read Online

ACCESS | Metrics & More | Article Recommendations | Supporting Information

ABSTRACT: Using time-lapsed ambient-pressure X-ray photoelectron spectroscopy, we investigate the thermal oxidation of single-crystalline Ir(100) films toward rutile IrO_2(110) in situ. We initially observe the formation of a carbon-free surface covered with a complete monolayer of oxygen, based on the binding energies of the Ir 4f and O 1s core level peaks. During a rather long induction period with nearly constant oxygen coverage, the work function of the surface changes continuously as sensed by the gas phase O 1s signal. The sudden and rapid formation of the IrO_2 rutile phase with a thickness above 3 nm, manifested by distinct binding energy changes and substantiated by quantitative XPS analysis, provides direct evidence that the oxide film is formed via an autocatalytic growth mechanism that was previously proposed for PbO and RuO_2.

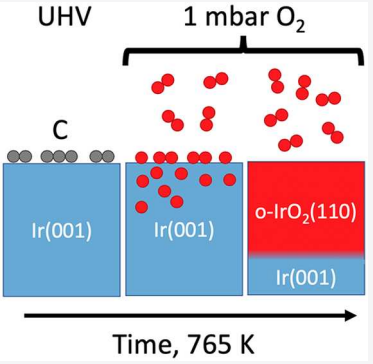

Iridium is the most corrosion-resistant metal, making it a suitable material for applications that require high reliability under extreme conditions, such as spark plugs in aviation engines, deep water pipes, or crucibles for evaporation sources. The oxides of Ir are known to be very stable electrode materials for the oxygen evolution reaction and were intensively studied by the electrochemical community in acidic media, including both thermally formed anhydrous oxide, as well as electrooxidized hydrous oxide.[1−5] While electrochemically formed hydrous iridium oxide is amorphous,[5] the thermally formed iridium oxide adopts the rutile structure, but the formation of such films requires oxygen pressures in the millibar range.[6,7] Such pressures are significantly higher than most surface sensitive, electron-based characterization techniques can tolerate, and given the difficulties with the controlled synthesis of rutile iridium oxides these materials were avoided by the surface science community for a long time. Recently, thermally grown IrO_2(110) films were found to be an excellent catalyst for low-temperature activation of methane,[8] which initiated an intense research focus on the chemistry and the properties of the IrO_2(110) surface.[6,9−12]

The (110)-oriented IrO_2 surface can be formed by thermal oxidation of Ir(100) substrates or by epitaxial growth of IrO_2 thin films on rutile-based substrates such as TiO_2(110)[13,14] or RuO_2(110)/Ru(0001).[15,16] While the epitaxially grown films demonstrate a better crystallinity compared to thermal oxidation, as observed using low-energy electron diffraction (LEED) and scanning tunneling microscopy (STM),[13−16] the preparation of such samples is rather time-consuming and a direct formation of the oxide film via thermal oxidation of Ir(100) is more desirable. Recently, the pressure dependence of the oxide growth, its structure, and the amount of oxygen within the oxide film were studied using LEED and temperature-programmed desorption. It was found that rotated IrO_2(110)R27° films can be grown by thermal oxidation of Ir(100) at 765 K and O_2 pressures of 0.75 Torr,[6] while aligned IrO_2(110) domains form upon oxidation using the same temperature at 5 Torr.[7] The structure of the oxides is well-known, but the kinetics of the oxide growth are still not well understood, calling for in situ studies with techniques such as ambient-pressure X-ray photoelectron spectroscopy (APXPS).

In this Letter, we report on the thermal oxidation of single-crystalline Ir(100) films in situ during time-lapsed APXPS measurements (see section S1 of the Supporting Information for experimental details). As received samples were inserted into the APXPS endstation (see overview spectrum in Figure S1), and all treatments included only thermal annealing in high vacuum (HV, 10^{-7} mbar) or 1 mbar of oxygen. During thermal oxidation, we observe a fast removal of carbon contamination, followed by a rather long induction period that leads to a rapid formation of the rutile IrO_2 phase within just a few minutes. Using quantitative analysis, we determine the stoichiometry of the formed oxide film and provide evidence that the oxide film

Received: March 23, 2020
Accepted: April 17, 2020
Published: April 17, 2020

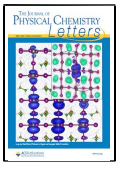

https://dx.doi.org/10.1021/acs.jpclett.0c00914
J. Phys. Chem. Lett. 2020, 11, 3601−3607

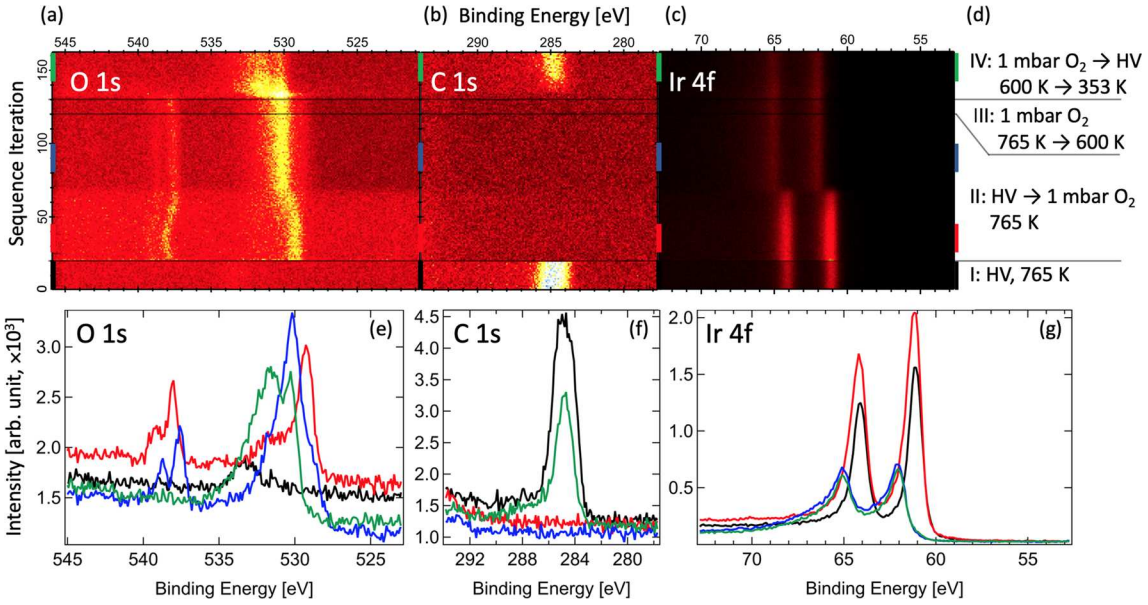

Figure 1. Time-lapse XPS spectra: (a–c) Sequence maps of O 1s, C 1s, and Ir 4f spectra acquired using a photon energy of 653 eV. Acquisition of O + C + Ir regions (one horizontal line in the plotted image) required 29.2 s per iteration. Panel (d) shows experimental conditions within the regions, with straight horizontal lines (extending through panels a–c) separating regions where the experimental conditions were changed. The lower part of the figure shows averages over 20 iterations for O 1s (e), C 1s (f), and Ir 4f (g) acquired at four different stages of the oxide formation process marked by the vertical colored bars separating the sequence maps: the black spectra (iterations 1–20) were acquired before oxygen was introduced to the high-pressure cell, and red (iterations 25–44) and blue (iteration 81–100) spectra in (e–g) were acquired at 1 mbar O_2 before and after the bulk iridium oxide film was formed, respectively. Spectra shown in green color were acquired during cooling down of the sample in high vacuum conditions (see iterations 142–161 in panels a–d). Fitting of the individual components for spectra shown in panels (e) and (g) is presented in Figure S2.

is formed via a self-catalytic growth mechanism that was previously proposed for PbO[17] and RuO_2.[18,19]

Figure 1 depicts the evolution of the O 1s, C 1s, and Ir 4f signals during the oxidation procedure at 765 K. Initially, in region I under HV and 765 K (iterations 1–20, see Figure 1d), we observe the Ir $4f_{7/2}$ peak at 61 eV which corresponds to metallic Ir,[20,21] and a pronounced C 1s peak at 284.8 eV that originates from adventitious carbon (see Figure 1e-g, spectra plotted in black). A weak oxygen signal is observed and is linked to the C-containing species on the surface (see black spectrum in Figure 1e). In region II (iterations 21–120), molecular oxygen is fed into the chamber at a pressure of 1 mbar while maintaining a constant temperature of 765 K. The carbon signal disappears immediately, concurrently with the appearance of the oxygen signals. The gas-phase O 1s signal shows up as a doublet of peaks (see red spectrum in Figure 1e),[22] initially at 538.1 and 539.2 eV, while a surface main component (α, see Figure S2a) is centered at 529.3 eV accompanied by a broad component (β, see Figure S2a) at 531.8 eV. In a discussion later in this letter, we will attribute these peaks to surface and subsurface oxygen atoms, respectively. At this time Ir still has its $4f_{7/2}$ peak centered at the metallic position (61.1 eV, see Figure 1g, red). After 48 iterations (corresponding to 23.5 min) in region II under constant pressure and temperature, a sudden change in the O 1s and Ir 4f spectra occurs. The Ir 4f peak changes to anhydrous IrO_2, which is represented by a main Ir $4f_{7/2}$ peak at 61.95 eV[21,23] (Figure 1g, blue) and can be fitted using procedures described in ref 21. The peak position and shape remain essentially unchanged for the rest of the experiment, as shown in regions III and IV (compare blue and green spectra in Figures 1g and S2b). In region III (iterations 121–130), the temperature was lowered to 600 K while maintaining a constant flux of O_2 into the high-pressure cell. This was done to avoid decomposition of the oxide film.[6] However, we observed a decrease of the total pressure to 0.86 mbar, which caused an increase of signal intensity due to reduced attenuation of photoelectrons in the gas phase (see region III in Figure 2a). Finally, in region IV (iterations 131–161), the heating was switched off and the high-pressure cell was evacuated to HV, resulting in a temperature of 353 K and pressure in the 10^{-7} mbar range at the end of the measurement.

Upon the sudden film transformation (at iteration 70 in Figure 1, corresponding to the time between minutes 32–34 in Figure 2), the shape of the surface O 1s peak also resembles that of anhydrous, rutile IrO_2 represented by an oxide peak at 530.1 eV and a satellite peak at 531.4 eV,[21] although the 529.3 eV peak is still present when the sample is at elevated temperature under oxidizing conditions (see Figure S2a). When the temperature is lowered below 600 K in region IV, this 529.3 eV O 1s peak disappears (see Figure 1e, green) and the C 1s signal starts to increase (Figure 1f, green). As a result of carbon buildup in region IV, the oxygen 1s signal is affected by additional components that are likely originating from the presence of residual carbon-containing gases and H_2O in the high-pressure cell.

To quantify the information contained in the spectra shown in Figure 1, we performed a numerical integration of background-corrected peaks for the O 1s, Ir 4f, and C 1s spectra. The results are shown in Figure 2a, where each point represents an average of five spectra divided by the respective photoionization cross section. These integrated peak intensities were then used for quantitative analysis. For small

https://dx.doi.org/10.1021/acs.jpclett.0c00914
J. Phys. Chem. Lett. 2020, 11, 3601–3607

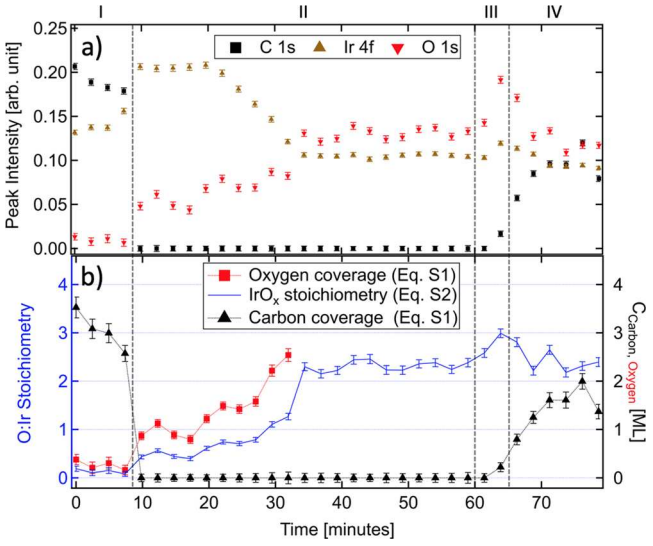

Figure 2. (a) Integrated intensities of the O 1s, Ir 4f, and C 1s signals from the as-measured data shown in Figure 1. Each point represents an average of five spectra that are divided by the respective cross sections. The time between adjacent points corresponds to ~2.5 min. Between minutes 10 and 62, the C 1s intensity is set to zero since there is no peak detectable in the as-measured XPS spectra when 1 mbar of oxygen is dosed at 765 K. Panel (b) contains the quantitative analysis of the coverage of carbon using the model of an ultrathin surface overlayer determined using eq S1. The same approach was used for the oxygen coverage in the initial stage of oxidation where the metallic substrate is still visible. After the formation of an anhydrous, rutile IrO_2 film (between minutes 32−34), the stoichiometry of the bulk oxide was determined using eq S2 and is plotted in blue in panel (b). Here, we used the model of an oxygen-rich, rutile $IrO_2(110)$ surface described in section S2 in the Supporting Information (SI).

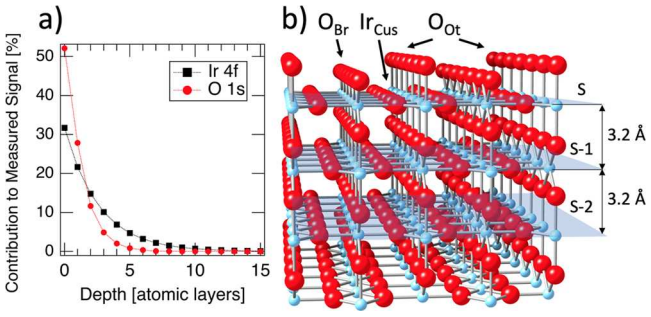

Figure 3. (a) Contribution of surface and subsurface oxygen and iridium atoms from oxygen-rich $IrO_2(110)$, shown as a ball and stick model in panel (b), to the measured intensities of the O 1s and Ir 4f signals excited with a photon energy of 653 eV. Zero depth covers the surface region that includes Ir and oxygen atoms present in the surface layer denoted with S, terminal oxygen atoms (O_{Ot}), and bridging oxygen atoms (O_{Br}). Emission from these surface atoms is assumed to not to be attenuated, while Ir and O emission in the subsurface region is assumed to be exponentially attenuated as described by eqs S3 and S4. Color coding in panel (b): oxygen atoms, red; iridium atoms, light blue.

coverages of oxygen (up to minute 32), we employed an ultrathin overlayer model (see ref 24 for more details) that is described by eq S1. The results in Figure 2b (red) show that the oxygen coverage between minutes 10 to 20 is around 1 monolayer (ML), which is here defined as one oxygen atom per one Ir atom on the (100)-terminated Ir surface. From minute 20 on, this coverage is higher than 1 ML, which is likely caused by the diffusion of O atoms into the subsurface, although this subsurface oxygen can also be related to the initial formation of the bulk oxide, such as 1D or 2D oxides or patches of suboxides with slightly different arrangements.[25] For later stages of the oxidation process, this ultrathin-film model (described by eq S1) is no longer applicable. The complete disappearance of the metallic Ir 4f signal indicates that the IrO_2 film is thicker than the probing depth of XPS using 653 eV photons. Time-resolved spectra shown in Figure 1 are very surface sensitive, with inelastic mean-free paths of $\lambda(E^{O}_{Kin})$ = 4.26 Å for O 1s and $\lambda(E^{Ir}_{Kin})$ = 9.73 Å for Ir 4f as calculated for electrons passing through IrO_2,[26] suggesting a film thickness above 2.9 nm (equivalent to 9 layers, see Figure 3b). This is in agreement with previous studies on the thermal oxidation of Ir(100) that reported the formation of a 3.5−6 nm thick $IrO_2(110)$ film when oxidized under similar conditions.[7,8] Interestingly, before the formation of the rutile IrO_2 film, we observe a linear decrease of the intensity of the Ir 4f peak between minutes 20 and 32 (see Figure 2a) while the intensity of the subsurface oxygen is increasing linearly (see Figure S3). Once the film transforms to rutile IrO_2 (as sensed from the metallic Ir 4f peak), the oxide thickness grows rapidly, since the intensity of the metallic Ir peak vanishes and the intensity of the O 1s peak instantly increases (see Figure 2, minutes 32−34). The amount of subsurface oxygen is by far not enough to form a thick rutile IrO_2 with a thickness above 3 nm (nine layers) but is still substantial. When considering the simplest possible model of the O−Ir−O trilayer structure, the amount of subsurface oxygen will correspond to an equivalent of 1.7 ML before IrO_2 formation (see Figure S3). The only plausible scenario for such a rapid increase in the thickness is that the presence of IrO_2 nuclei enhances the dissociation probability of O_2 molecules impinging on the surface (compared to oxygen-terminated Ir(100) surface), that was indeed proposed to be the mechanism of the self-catalyzed growth mechanism.[18]

To quantify the composition of the Ir oxide film formed in the region after minute 34 (Figure 2), we used a model of oxygen-rich $IrO_2(110)$ that is shown in Figure 3b. Such a surface is fully saturated with terminal oxygen atoms (O_{Ot}) that are placed on top of normally coordinatively unsaturated surface iridium atoms (Ir_{Cus}). Because of the low photon energy used (653 eV), the contribution of surface atoms to the measured peak intensity is significant. For O 1s, roughly 50% of the measured peak intensity originates from the O_{Ot}, bridging oxygen atoms (O_{Br}), and oxygen atoms within the surface layer (S), while over 90% of the measured signal originates from the surface (S) and the first two subsurface layers (S-1 and S-2, see Figure 3a). For Ir 4f, the surface iridium atoms contribute about 32% to the measured intensity with 90% of the measured signal originating from the region reaching down to the fifth subsurface layer. The equations used to derive the plot in Figure 3a are described in section S2 in the SI. The stoichiometry of the bulk iridium oxide was then determined using a model of a homogeneous binary oxide (see section S2, SI) corrected by the contributions of the individual atomic layers to the measured signal (see Figure 3a). This yielded an average 2.3 ± 0.1 atomic ratio between oxygen and iridium within the bulk iridium oxide film (see blue data points in Figure 2b after minute 34). If a model of stoichiometric $IrO_2(110)$ is used instead, the calculated average atomic ratio is 2.8 ± 0.1, which is unrealistic. Thus, the model of oxygen-rich $IrO_2(110)$ was chosen since the surface is expected to be

https://dx.doi.org/10.1021/acs.jpclett.0c00914
J. Phys. Chem. Lett. 2020, 11, 3601−3607

O_{Ot}-terminated as long as the sample is exposed to 1 mbar of O_2.[10,27] The resulting ratio is still slightly higher than the expected 2:1 oxygen to iridium ratio in IrO_2 which can be caused by a number of effects, such as, e.g., X-ray photoelectron diffraction (XPD) effects.[24] For example, our previous XPD measurements on an isomorphic rutile $RuO_2(110)$ surface showed azimuthal intensity modulations of 15% for O 1s and 5% for Ru 3d for a polar emission angle of 30°. Another effect is that in eq S3 the top Ir layer is not attenuated ($n = 0$), while this layer is still covered by O_{Br} and O_{Ot}. This attenuation would reduce the relative contribution, r_{Ir}, of Ir to the measured intensity, and this will reduce the O:Ir ratio further toward the expected 2:1 ratio.

During the oxidation process, the peak shapes and positions for metallic Ir (black spectra in Figure 1e and g) and as-grown IrO_2 (blue spectra in Figure 1e and g) agree well with previously reported literature spectra for metallic iridium and rutile IrO_2, respectively.[21] The latter exhibits strongly asymmetric line shapes due to the many-body screening response of the 5d conducting electrons.[28] We find an uncommon peak position for O 1s in region II before the bulk oxide film is formed (while the sample is exposed to 1 mbar of O_2 at 765 K, see Figure 1e, red), where the main peak (α, see Figure S2a) is centered at 529.3 eV, a value lower by 0.5 eV than the typical binding energy of 529.8 ± 0.2 eV reported for chemisorbed oxygen on Ir(111) or oxygen in IrO_2.[13,15,21,29−31] This peak can be fitted with a single Gaussian−Lorentzian function (see Table S1), and it is attributed to chemisorbed oxygen in the bridging configuration before the rutile oxide film is formed[32] and to O_{Br} after IrO_2 formation. The broad peak is tentatively assigned to subsurface oxygen (see Figures S2 and S3 and their corresponding captions for a rationalization of these peak assignments).

While chemisorbed oxygen on Ir(100) was studied extensively by techniques such as LEED or STM,[33−35] the number of O 1s spectra published for this surface is limited.[32,36] For coverages up to 0.5 ML, oxygen adapts a bridging site configuration, eventually forming a (2 × 1)-O reconstruction that is stable up to 740 K.[33] In XPS, the binding energy of O 1s is shifted by −0.5 eV compared to Ir(111),[32] which is attributed to adsorption of oxygen on the bridging sites of the Ir(100) surface compared to the threefold hollow sites on Ir(111). Only very little is known for chemisorbed oxygen on Ir(100) at coverages above 0.5 ML. When the oxygen coverage is between 0.5 and 0.75 ML, compressive stress distorts the surface. For these coverages, it is predicted that oxygen is present both in bridge and hollow sites,[37] and the desorption temperature of oxygen is expected to be lower due to the repulsive interactions between adsorbed oxygen atoms,[33] although this preference for the hollow site occupation was questioned in later studies.[38,39] Moreover, chemisorbed (2 × 1)-O/Ir(100) undergoes a reversible order−disorder transition above 650 K,[33] as was demonstrated for the (2 × 1)-O phase, where the fractional spots vanished between 620 and 680 K. This transition was shown to be reversible with a small hysteresis (<10 K), and it is likely linked to the enhancement of the surface diffusion of adsorbed oxygen at temperatures above 650 K.[34] For the O 1s spectrum shown in Figure 1e (red), we find that the total oxygen coverage is 1 ML and the signal consists of 2/3 of a ML of surface chemisorbed oxygen[32] with the remaining equivalent of 1/3 ML of oxygen atoms located in the subsurface region[40] (see Figures S2 and S3). The underlying iridium still maintains its metallic character, as indicated by the Ir 4f spectrum (see Figures 1g and S2b). Fitting of the Ir 4f spectra reveals that, upon surface saturation with chemisorbed oxygen, the Ir 4f peak shifts by +100 meV binding energy and the fwhm increases slightly (see Figure S2 and Table S2). Similar core-level behavior was observed previously for chemisorbed and subsurface oxygen on Ir(111)[41] and Ru(0001).[42] To our knowledge, this is the first experimental evidence showing chemisorbed oxygen on Ir(100) at a coverage above 0.5 ML. However, more work is required to learn about the adsorption structure, stability, and reactivity of high coverages of oxygen on Ir(100).

Finally, we conclude this discussion by addressing the sudden IrO_2 oxide formation, which can be observed by following the Ir 4f core level signal (see Figure 1c). The metal to oxide transition occurs almost instantly (between iteration 65−70, corresponding to minute 32−34), following a rather long induction period. This metal to oxide transition shows a very fast growth kinetics and the most plausible explanation is to assign this to self-catalytic oxide growth, where upon the formation of IrO_2 nuclei the oxide growth is strongly enhanced. Similar growth was previously proposed for Ru(0001) to $RuO_2(110)$ oxidation, and this mechanism was verified by surface X-ray diffraction studies.[18,19]

Interestingly, we can sense changes in the work function of the metallic Ir substrate during this induction period. The work function first slightly decreases and then later increases, which results in an initial shift of the gas phase O 1s peak toward higher binding energy, followed by a second, larger shift to lower binding energy (see Figure S3).[43] During the initial work function decrease (iteration 21−40), we see an almost constant coverage of both chemisorbed oxygen and subsurface oxygen (see Figure S3). When the work function starts to increase, we see a simultaneous increase of the amount of accumulated subsurface oxygen (see peak β in Figure S3, iteration 41−65). To understand this work function change, one has to refer to different surface terminations that can occur during the oxidation of Ir(100) toward IrO_2. For clean Ir(100), two different reconstructions are known with essentially the same work function (ϕ) determined experimentally: for the (5 × 1) reconstruction, $\phi = 5.95 \pm 0.25$ eV, and for Ir(100)-(1 × 1), $\phi = 5.97 \pm 0.23$ eV.[44] Density functional theory studies predict a linear increase of the work function with increasing coverage of chemisorbed oxygen in the 0−1 ML range.[38,39] Such an increase is related to partial electron transfer from iridium surface atoms to oxygen adatoms, caused by the large difference in electronegativities between oxygen (3.44) and iridium (2.20), that yields a surface dipole layer.

At our experimental conditions, the surface is immediately in a high coverage regime as soon as 1 mbar of oxygen is admitted into the chamber (Figure S3). A reliable experimental value for the work function of rutile IrO_2 or Ir(100) with subsurface oxygen is not available. Making the analogy with similar systems such as Ru(0001) does not help to explain this work function behavior, since for oxygen-saturated Ru(0001), where oxygen atoms are forming a (1 × 1)-O overlayer, the surface dipole layer reaches its maximum strength and the work function the highest value compared to the clean Ru(0001) surface.[45,46] For higher coverages of oxygen, attributed to oxygen incorporation into the subsurface region, the work function decreases by about 0.3−0.7 eV, depending on the temperature during oxygen exposure.[45,46] The behavior of the work function in the Ir−rO_2 system, as probed by the gas phase O 1s peak (see Figure S3), shows an exactly opposite

https://dx.doi.org/10.1021/acs.jpclett.0c00914
J. Phys. Chem. Lett. 2020, 11, 3601−3607

trend: with a slight increase of the coverage of chemisorbed oxygen on the Ir(100) surface, the position of the gas-phase O 1s peak moves toward higher binding energy (corresponding to decreasing work function), and when the coverage of subsurface oxygen starts to increase (blue curve in Figure S3), the gas phase peak moves toward lower binding energy (increasing work function). The shift of the gas-phase O 1s peak could in principle be caused by other effects than work function change, such as charging, but since both Ir and IrO_2 are metallic, we can exclude this possibility.[43,47,48] We hypothesize that this unique behavior is caused by oxygen-induced roughening of the surface in the initial phase (iteration 21−40), when the surface is initially sealed but undergoes roughening due to interaction with oxygen at elevated temperatures, as observed previously during initial stages of oxidation of Ir(111).[25] The sign for significant surface roughening is supported by rather blurry IrO_2(110) LEED patterns reported previously under similar conditions,[7] which indicates that thermally oxidized Ir(100) is likely not a good model system to study IrO_2(110). The work function increase during the accumulation of subsurface oxygen (see iteration 41−65 in Figure S3) is even more surprising and will require structure-sensitive techniques capable of operation in the mbar pressure range, such as high energy surface X-ray diffraction, to address possible structural changes of the metallic Ir during the induction period preceding the formation of a rutile IrO_2 film.

In this Letter, we monitored the formation of rutile IrO_2(110) in situ during thermal oxidation of Ir(100). During the oxidation process at 1 mbar of O_2 at 765 K, we observe first a saturation of the surface with chemisorbed oxygen, followed by a linear increase in the intensity of the O 1s peak representing subsurface oxygen atoms, concurrently with a linear decrease of the intensity of the metallic Ir 4f signal. Once a critical concentration of subsurface oxygen was reached, the film transformed spontaneously and very rapidly into the rutile IrO_2(110) structure. The presence of rutile IrO_2 islands greatly accelerates the dissociation of oxygen and leads to a sudden increase of the oxygen content. This results in an increase of the thickness of the IrO_2 film and the disappearance of the metallic Ir 4f signal from the underlying Ir(100) film. In this study, we observe this kind of autocatalytic growth mode for the first time using APXPS. Our findings demonstrate the strength of APXPS to study adsorption and reaction mechanisms, such as in situ oxidation of 4d and 5d transition metals that often require high oxygen pressures at elevated temperatures.

■ ASSOCIATED CONTENT

Supporting Information

The Supporting Information is available free of charge at https://pubs.acs.org/doi/10.1021/acs.jpclett.0c00914.

Detailed description of experimental details; formulas used for quantification of XPS spectra; survey XPS spectrum for the as-inserted Ir(100) sample; peak fitting of the spectra shown in Figure 1e,g and fitting parameters used; graph showing time evolution of the intensity of surface and subsurface oxygen on Ir(100) before the formation of the rutile oxide film; energy position of gas-phase O $1s_{3/2}$ (PDF)

■ AUTHOR INFORMATION

Corresponding Authors

Zbynek Novotny − *Physik-Institut, Universität Zürich, CH-8057 Zürich, Switzerland; Swiss Light Source, Paul Scherrer Institut, CH-5232 Villigen-PSI, Switzerland;* orcid.org/0000-0002-3575-7535; Email: zbynek.novotny@psi.ch

Jürg Osterwalder − *Physik-Institut, Universität Zürich, CH-8057 Zürich, Switzerland;* orcid.org/0000-0001-9517-641X; Email: osterwal@physik.uzh.ch

Authors

Benjamin Tobler − *Physik-Institut, Universität Zürich, CH-8057 Zürich, Switzerland*

Luca Artiglia − *Swiss Light Source, Paul Scherrer Institut, CH-5232 Villigen-PSI, Switzerland;* orcid.org/0000-0003-4683-6447

Martin Fischer − *Institut für Physik, Universität Augsburg, D-86135 Augsburg, Germany*

Matthias Schreck − *Institut für Physik, Universität Augsburg, D-86135 Augsburg, Germany*

Jörg Raabe − *Swiss Light Source, Paul Scherrer Institut, CH-5232 Villigen-PSI, Switzerland;* orcid.org/0000-0002-2071-6896

Complete contact information is available at: https://pubs.acs.org/10.1021/acs.jpclett.0c00914

Notes

The authors declare no competing financial interest.

■ ACKNOWLEDGMENTS

This work was performed at the In Situ Spectroscopy (X07DB) beamline of the Swiss Light Source, Paul Scherrer Institut, Villigen PSI, Switzerland, using the Solid−Gas Interface Chamber (SGIC). We thank Jason F. Weaver, Markus Ammann, Anthony Boucly, and Thomas Greber for fruitful discussions and J. Trey Diulus and Nicolo Comini for proofreading the final version of the Letter. We acknowledge financial support from the Swiss National Science Foundation under the Grants 206021_170747 and 200020_172641.

■ REFERENCES

(1) Steegstra, P.; Busch, M.; Panas, I.; Ahlberg, E. Revisiting the Redox Properties of Hydrous Iridium Oxide Films in the Context of Oxygen Evolution. *J. Phys. Chem. C* **2013**, *117* (40), 20975−20981.

(2) Geiger, S.; Kasian, O.; Shrestha, B. R.; Mingers, A. M.; Mayrhofer, K. J. J.; Cherevko, S. Activity and Stability of Electrochemically and Thermally Treated Iridium for the Oxygen Evolution Reaction. *J. Electrochem. Soc.* **2016**, *163* (11), F3132−F3138.

(3) Saveleva, V. A.; Wang, L.; Teschner, D.; Jones, T.; Gago, A. S.; Friedrich, K. A.; Zafeiratos, S.; Schlögl, R.; Savinova, E. R. Operando Evidence for a Universal Oxygen Evolution Mechanism on Thermal and Electrochemical Iridium Oxides. *J. Phys. Chem. Lett.* **2018**, *9* (11), 3154−3160.

(4) Pfeifer, V.; Jones, T. E.; Velez, J. J. V.; Massue, C.; Greiner, M. T.; Arrigo, R.; Teschner, D.; Girgsdies, F.; Scherzer, M.; Allan, J.; Hashagen, M.; Weinberg, G.; Piccinin, S.; Havecker, M.; Knop-Gericke, A.; Schlogl, R. The electronic structure of iridium oxide electrodes active in water splitting. *Phys. Chem. Chem. Phys.* **2016**, *18* (4), 2292−2296.

(5) Pfeifer, V.; Jones, T. E.; Velasco Vélez, J. J.; Arrigo, R.; Piccinin, S.; Hävecker, M.; Knop-Gericke, A.; Schlögl, R. In situ observation of reactive oxygen species forming on oxygen-evolving iridium surfaces. *Chemical Science* **2017**, *8* (3), 2143−2149.

(6) Li, T.; Kim, M.; Liang, Z.; Asthagiri, A.; Weaver, J. F. Dissociative Chemisorption and Oxidation of H_2 on the Stoichiometric IrO_2(110) Surface. *Top. Catal.* **2018**, *61* (5), 397−411.
(7) Bian, Y.; Li, T.; Weaver, J. F. Structure and reactivity of iridium oxide layers grown on Ir(100) by oxidation at sub-ambient O_2 pressures. *J. Phys. D: Appl. Phys.* **2019**, *52* (43), 434002.
(8) Liang, Z.; Li, T.; Kim, M.; Asthagiri, A.; Weaver, J. F. Low-temperature activation of methane on the IrO_2(110) surface. *Science* **2017**, *356* (6335), 299.
(9) Bian, Y.; Kim, M.; Li, T.; Asthagiri, A.; Weaver, J. F. Facile Dehydrogenation of Ethane on the IrO_2(110) Surface. *J. Am. Chem. Soc.* **2018**, *140* (7), 2665−2672.
(10) Li, T.; Kim, M.; Liang, Z.; Asthagiri, A.; Weaver, J. F. Hydrogen oxidation on oxygen-rich IrO_2(110). *Catalysis, Structure & Reactivity* **2018**, *4* (4), 1−13.
(11) Tsuji, Y.; Yoshizawa, K. Adsorption and Activation of Methane on the (110) Surface of Rutile-type Metal Dioxides. *J. Phys. Chem. C* **2018**, *122* (27), 15359−15381.
(12) Martin, R.; Kim, M.; Franklin, A.; Bian, Y.; Asthagiri, A.; Weaver, J. F. Adsorption and oxidation of propane and cyclopropane on IrO_2(110). *Phys. Chem. Chem. Phys.* **2018**, *20* (46), 29264−29273.
(13) Abb, M. J. S.; Weber, T.; Glatthaar, L.; Over, H. Growth of Ultrathin Single-Crystalline IrO_2(110) Films on a TiO_2(110) Single Crystal. *Langmuir* **2019**, *35* (24), 7720−7726.
(14) Kuo, D.-Y.; Kawasaki, J. K.; Nelson, J. N.; Kloppenburg, J.; Hautier, G.; Shen, K. M.; Schlom, D. G.; Suntivich, J. Influence of Surface Adsorption on the Oxygen Evolution Reaction on IrO_2(110). *J. Am. Chem. Soc.* **2017**, *139* (9), 3473−3479.
(15) Abb, M. J. S.; Herd, B.; Over, H. Template-Assisted Growth of Ultrathin Single-Crystalline IrO_2(110) Films on RuO_2(110)/Ru-(0001) and Its Thermal Stability. *J. Phys. Chem. C* **2018**, *122* (26), 14725−14732.
(16) Weber, T.; Pfrommer, J.; Abb, M. J. S.; Herd, B.; Khalid, O.; Rohnke, M.; Lakner, P. H.; Evertsson, J.; Volkov, S.; Bertram, F.; Znaiguia, R.; Carla, F.; Vonk, V.; Lundgren, E.; Stierle, A.; Over, H. Potential-Induced Pitting Corrosion of an IrO_2(110)-RuO_2(110)/Ru(0001) Model Electrode under Oxygen Evolution Reaction Conditions. *ACS Catal.* **2019**, *9* (7), 6530−6539.
(17) Thürmer, K.; Williams, E.; Reutt-Robey, J. Autocatalytic Oxidation of Lead Crystallite Surfaces. *Science* **2002**, *297* (5589), 2033.
(18) He, Y. B.; Knapp, M.; Lundgren, E.; Over, H. Ru(0001) Model Catalyst under Oxidizing and Reducing Reaction Conditions: In-Situ High-Pressure Surface X-ray Diffraction Study. *J. Phys. Chem. B* **2005**, *109* (46), 21825−21830.
(19) Over, H.; Seitsonen, A. P. Oxidation of Metal Surfaces. *Science* **2002**, *297* (5589), 2003−2005.
(20) Moulder, J.; Chastain, J.; King, R. *Handbook of X-ray Photoelectron Spectroscopy: a reference book of standard spectra for identification and interpretation of XPS data*; Physical Electronics, 1995.
(21) Freakley, S. J.; Ruiz-Esquius, J.; Morgan, D. J. The X-ray photoelectron spectra of Ir, IrO_2 and $IrCl_3$ revisited. *Surf. Interface Anal.* **2017**, *49* (8), 794−799.
(22) Siegbahn, K. Electron spectroscopy for atoms, molecules, and condensed matter. *Rev. Mod. Phys.* **1982**, *54* (3), 709−728.
(23) Peuckert, M. XPS study on thermally and electrochemically prepared oxidic adlayers on iridium. *Surf. Sci.* **1984**, *144* (2−3), 451−464.
(24) Osterwalder, J., Electron Based Methods: 3.2.2 Photoelectron Spectroscopy and Diffraction. In *Surface and Interface Science*; Wiley-VCH Verlag GmbH & Co. KGaA: 2014; pp 151−214.
(25) He, Y. B.; Stierle, A.; Li, W. X.; Farkas, A.; Kasper, N.; Over, H. Oxidation of Ir(111): From O−Ir−O Trilayer to Bulk Oxide Formation. *J. Phys. Chem. C* **2008**, *112* (31), 11946−11953.
(26) Tanuma, S.; Powell, C. J.; Penn, D. R. Calculations of electron inelastic mean free paths. V. Data for 14 organic compounds over the 50−2000 eV range. *Surf. Interface Anal.* **1994**, *21* (3), 165−176.
(27) Chung, W.-H.; Wang, C.-C.; Tsai, D.-S.; Jiang, J.-C.; Cheng, Y.-C.; Fan, L.-J.; Yang, Y.-W.; Huang, Y.-S. Deoxygenation of IrO_2(110) surface: Core-level spectroscopy and density functional theory calculation. *Surf. Sci.* **2010**, *604* (2), 118−124.
(28) Wertheim, G. K.; Guggenheim, H. J. Conduction-electron screening in metallic oxides: IrO_2. *Phys. Rev. B: Condens. Matter Mater. Phys.* **1980**, *22* (10), 4680−4683.
(29) Johansson, N.; Andersen, M.; Monya, Y.; Andersen, J. N.; Kondoh, H.; Schnadt, J.; Knudsen, J. Ambient pressure phase transitions over Ir(111): at the onset of CO oxidation. *J. Phys.: Condens. Matter* **2017**, *29* (44), 444002.
(30) Zhdan, P. A.; Boreskov, G. K.; Boronin, A. I.; Egelhoff, W. F.; Weinberg, W. H. An XPS investigation of the chemisorption of oxygen on the iridium (111) surface. *Surf. Sci.* **1976**, *61* (1), 25−36.
(31) Cassidy, A.; Pedersen, S.; Bluhm, H.; Calisti, V.; Angot, T.; Salomon, E.; Bisson, R.; Hornekær, L. Patterned formation of enolate functional groups on the graphene basal plane. *Phys. Chem. Chem. Phys.* **2018**, *20*, 28370.
(32) Arman, M.; Knudsen, J.; Gustafson, J.; Ferstl, P.; Mittendorfer, F.; Lundgren, E., Stable and metastable Ir(100) surface structures studied with X-ray photoelectron spectroscopy. In *IVC-19*, Paris, France, 2013.
(33) Ferstl, P.; Schmitt, T.; Schneider, M. A.; Hammer, L.; Michl, A.; Müller, S. Structure and ordering of oxygen on unreconstructed Ir(100). *Phys. Rev. B: Condens. Matter Mater. Phys.* **2016**, *93* (23), 235406.
(34) Ali, T.; Klötzer, B.; Walker, A. V.; Ge, Q.; King, D. A. Surface kinetics of a nonlinear oxygen-induced $(1 \times 5) \rightarrow (1 \times 1)$ phase transition on Ir{100}. *J. Chem. Phys.* **1998**, *109* (22), 9967−9976.
(35) Johnson, K.; Ge, Q.; Titmuss, S.; King, D. A. Unusual bridged site for adsorbed oxygen adatoms: Theory and experiment for Ir{100}−(1×2)−O. *J. Chem. Phys.* **2000**, *112* (23), 10460−10466.
(36) Anic, K.; Bukhtiyarov, A. V.; Li, H.; Rameshan, C.; Rupprechter, G. CO Adsorption on Reconstructed Ir(100) Surfaces from UHV to mbar Pressure: A LEED, TPD, and PM-IRAS Study. *J. Phys. Chem. C* **2016**, *120* (20), 10838−10848.
(37) Sander, D.; Meyerheim, H. L.; Tian, Z.; Niebergall, L.; Negulyaev, N. N.; Mohseni, K.; Stepanyuk, V. S.; Felici, R.; Kirschner, J. Sequential population of adsorption sites driven by surface stress. *Phys. Rev. B: Condens. Matter Mater. Phys.* **2010**, *81* (15), 153403.
(38) Erikat, I. A.; Hamad, B. A.; Khalifeh, J. M. Adsorption of O and CO on Ir(100) from first principles. *Eur. Phys. J. B* **2009**, *67* (1), 35−41.
(39) Ma, S. H.; Jiao, Z. Y.; Zhang, X. Z.; Yang, Z. X.; Dai, X. Q. A density functional theory study of ordered oxygen overlayers on Ir(100). *Eur. Phys. J. B* **2012**, *85* (6), 216.
(40) Wider, J.; Greber, T.; Wetli, E.; Kreutz, T. J.; Schwaller, P.; Osterwalder, J. Direct observation of subsurface oxygen on Rh(111). *Surf. Sci.* **1998**, *417* (2), 301−310.
(41) Marinova, T. S.; Kostov, K. L. Interaction of oxygen with a clean Ir(111) surface. *Surf. Sci.* **1987**, *185* (1), 203−212.
(42) Malik, I. J.; Hrbek, J. Very high atomic oxygen coverages on Ru(001). *J. Vac. Sci. Technol., A* **1992**, *10* (4), 2565−2569.
(43) Axnanda, S.; Scheele, M.; Crumlin, E.; Mao, B.; Chang, R.; Rani, S.; Faiz, M.; Wang, S.; Alivisatos, A. P.; Liu, Z. Direct Work Function Measurement by Gas Phase Photoelectron Spectroscopy and Its Application on PbS Nanoparticles. *Nano Lett.* **2013**, *13* (12), 6176−6182.
(44) Derry, G. N.; Kern, M. E.; Worth, E. H. Recommended values of clean metal surface work functions. *J. Vac. Sci. Technol., A* **2015**, *33* (6), 060801.
(45) Blume, R.; Niehus, H.; Conrad, H.; Böttcher, A. Oxide-free oxygen incorporation into Ru(0001). *J. Chem. Phys.* **2004**, *120* (8), 3871−3879.
(46) Bottcher, A.; Niehus, H. Oxygen adsorbed on oxidized Ru(0001). *Phys. Rev. B: Condens. Matter Mater. Phys.* **1999**, *60* (20), 14396−14404.
(47) Lampimäki, M.; Schreiber, S.; Zelenay, V.; Křepelová, A.; Birrer, M.; Axnanda, S.; Mao, B.; Liu, Z.; Bluhm, H.; Ammann, M. Exploring the Environmental Photochemistry on the TiO_2(110)

https://dx.doi.org/10.1021/acs.jpclett.0c00914
J. Phys. Chem. Lett. 2020, 11, 3601−3607

Surface in Situ by Near Ambient Pressure X-ray Photoelectron Spectroscopy. *J. Phys. Chem. C* **2015**, *119* (13), 7076−7085.
(48) Naitabdi, A.; Boucly, A.; Rochet, F.; Fagiewicz, R.; Olivieri, G.; Bournel, F.; Benbalagh, R.; Sirotti, F.; Gallet, J.-J. CO oxidation activity of Pt, Zn and ZnPt nanocatalysts: a comparative study by in situ near-ambient pressure X-ray photoelectron spectroscopy. *Nanoscale* **2018**, *10* (14), 6566−6580.

https://dx.doi.org/10.1021/acs.jpclett.0c00914
J. Phys. Chem. Lett. 2020, 11, 3601−3607